THE JOURNAL OF PHYSICAL CHEMISTRY C

Article

pubs.acs.org/JPCC

Synchrotron Diffraction Studies of Hydrogen Absorption/Desorption on $CaH_2 + MgB_2$ Reactive Hydride Composite Mixed With Fluorinated Compounds

K. Suarez-Alcantara,*[,†,‡] M. H. Sørby,[§] C. Pistidda,[‡] F. Karimi,[‡] I. Saldan,[‡,∥] B. C. Hauback,[§] T. Klassen,[‡] and M. Dornheim[‡]

[†]Unidad Morelia del Instituto de Investigaciones en Materiales, Universidad Nacional Autónoma de México, Antigua Carretera a Pátzcuaro No. 8701, Col. Ex Hacienda de San José de la Huerta, C.P. 58190, Morelia, Michoacán, México

[‡]Institute of Materials Research, Materials Technology, Helmholtz-Zentrum Geesthacht, D-21502, Geesthacht, Germany

[§]Institute for Energy Technology (IFE), P.O. Box 40, NO-2027 Kjeller, Norway

[∥]Department of Physical and Colloid Chemistry, Ivan Franko National University of Lviv, Kyryla and Mefodia St. 6, 79005 Lviv, Ukraine

ABSTRACT: The reactive hydride composites $9CaH_2 + CaF_2 + 10MgB_2$, $10Ca(BH_4)_2 + 9MgH_2 + MgF_2$, and $9Ca(BH_4)_2 + Ca(BF_4)_2 + 10MgH_2$ were prepared by ball milling. Their properties toward hydrogen absorption/desorption were tested by means of manometric measurements. The highest hydrogen storage capacity was obtained for $9CaH_2 + CaF_2 + 10MgB_2$ (7.6 wt %) at the first cycle. The effects of CaF_2, MgF_2, or $Ca(BF_4)_2$ on the dehydrogenation reaction were studied by means of in situ synchrotron radiation powder X-ray diffraction (in situ SR-PXD) and differential scanning calorimetry (DSC). The high resolution SR-PXD technique was used to confirm the formation of hydrogenated products and side products in the $9CaH_2 + CaF_2 + 10MgB_2$ reactive hydride composites. These studies indicate the formation of a complex mixture of phases.

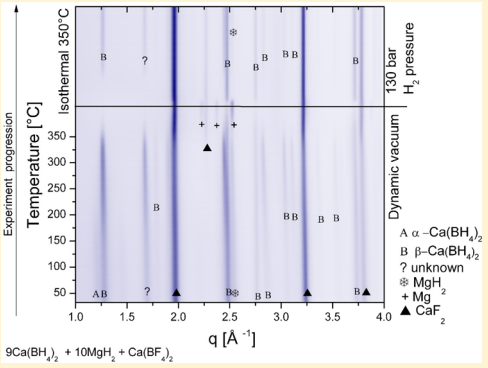

1. INTRODUCTION

Hydrogen storage technology is of critical importance to the implementation of polymer electrolyte membrane fuel cell (PEMFC) driven electric vehicles. Among the most important characteristics for tangible hydrogen storage is the hydrogen absorption/desorption reaction enthalpy. It has been proposed an enthalpy target range of 25−50 kJ mol^{-1} H_2 ,[1,2] i.e., P_{eq} = 1 bar and between approximately −45 and 150 °C. These temperature limits represent the cold PEMFC starting and a typical high temperature polymer electrolyte membrane fuel cell (HT-PEMFC) operation.[3,4] The reactive hydride composites (RHCs) have been proposed as an alternative to tailor the hydrogen desorption enthalpy.[5,6] In the RHC, the overall hydrogen desorption enthalpy per mole of hydrogen is lowered compared with those of the single components of the mixture.[5,6] Among the RHCs, the system

$$Ca(BH_4)_2 + MgH_2 \leftrightarrow CaH_2 + MgB_2 + 4H_2$$
$$8.4\ \text{wt \% of } H_2 \text{ storage} \qquad (1)$$

has been proposed as a potential system for hydrogen storage.[7] The reaction enthalpy calculated for eq 1 is $\Delta H^{T=300K}$ = 47.0 kJ mol^{-1} H_2, which entails an equilibrium pressure of 1 bar at 135 °C.[8] However, activation energy, kinetics, reaction pathway, formation of side products, low reversibility, etc., prevent reaction 1 from proceeding as depicted. A wide range of additives have been shown to enhance reversibility or to increase hydriding/dehydriding kinetics in borohydride mixtures, especially materials based on transition metals like Ti, Zr, and Nb.[9] Fluorinated compounds have been studied as additives to improve the hydriding/dehydriding properties of calcium borohydride,[10] where materials such as TiF_4 and NbF_5 improved the rehydrogenation reaction.[10] Similarities in structure and chemistry of fluorides versus hydrides have suggested the possibility of their use as reaction-pathway modifiers.[11−14] Lee et al.[15] proposed that CaF_2 interacts with $Ca(BH_4)_2$ and drives the decomposition by forming $Ca(H_{1-y}F_y)_2$ and CaB_6. MgF_2 in the $Ca(BH_4)_2 + MgF_2$ mixture[16] or CaF_2 in $3CaH_2 + CaF_2 + 4MgB_2$[17−19] has been used to modify the pathway of reaction 1. Following with the similarities in structure or chemistry, the mixtures $9CaH_2 + CaF_2 + 10MgB_2$, $10Ca(BH_4)_2 + 9MgH_2 + MgF_2$, and $9Ca(BH_4)_2 + Ca(BF_4)_2 + 10MgH_2$ were prepared and studied for hydrogen storage applications in the presented work.

Received: February 27, 2015
Revised: April 24, 2015
Published: May 8, 2015

DOI: 10.1021/acs.jpcc.5b01961
J. Phys. Chem. C 2015, 119, 11430−11437

2. EXPERIMENTAL DETAILS

2.1. Reactive Hydride Composite Preparation. The following Ca-based RHCs were prepared by high energy ball milling: (a) $9CaH_2 + CaF_2 + 10MgB_2$, (b) $10Ca(BH_4)_2 + 9MgH_2 + MgF_2$, and (c) $9Ca(BH_4)_2 + Ca(BF_4)_2 + 10MgH_2$. All chemicals were purchased from Sigma-Aldrich; purities: CaH_2 95%, CaF_2 99.99%, MgH_2 99.99%, MgF_2 99.99%, $Ca(BH_4)_2{\cdot}2THF$ 95%, and $Ca(BF_4)_2{\cdot}xH_2O$ 95%. The as-received $Ca(BF_4)_2{\cdot}xH_2O$ was dried at 110 °C and under a dynamic vacuum for 3 h in order to eliminate H_2O. The as-received $Ca(BH_4)_2{\cdot}2THF$ was dried at 190 °C and under a dynamic vacuum for 3 h in order to eliminate THF. The rest of the materials were used as received.

Ball milling was performed in two stages. In the first stage, the fluorinated compound and the corresponding hydrogenated compound, i.e., CaF_2/CaH_2, MgH_2/MgF_2, or $Ca(BH_4)_2/Ca(BF_4)_2$, were milled together for 60 h. In the second stage, the resulting mixture and MgB_2, $Ca(BH_4)_2$, or MgH_2, respectively, were milled together for a further 27 h. The ball milling process was performed in a SPEX 8000 miller. The ball to powder ratio was kept as 10:1. The vial material was stainless steel, the ball material was ceramic zirconium oxide, and no process agent control was used. All powder handling and milling processes were carried out in an MBraun argon-filled glovebox. The H_2O and O_2 concentration was kept below 10 ppm. Additionally, $Ca(BH_4)_2 + MgH_2$ and $CaH_2 + MgB_2$ mixtures were prepared by 27 h of ball milling; these materials and CaF_2/CaH_2 or MgH_2/MgF_2 ball milled mixtures are presented as references.

2.2. Hydrogen Absorption/Desorption Testing. Hydrogen absorption/desorption experiments were carried out in a PCTPro-2000 SETARAM instrument. During the first absorption/desorption, the applied temperature and hydrogen pressure conditions were 350 °C and 130 bar H_2 pressure for the absorption; meanwhile, desorption was performed at 350 °C and 0.1 bar H_2 pressure. This experimental condition was applied for all three studied composites.

Due to the acceptable hydrogen uptake of $9CaH_2 + CaF_2 + 10MgB_2$ (see below), this material was cycled one additional time under the same conditions as the first cycle and characterized by high resolution SR-PXD in each stage of hydrogen absorption/desorption.

2.3. In Situ and High Resolution SR-PXD. Samples of hydrogenated $9CaH_2 + CaF_2 + 10MgB_2$ (hereafter as $9CaH_2 + CaF_2 + 10MgB_2 - 1ab$), the as-milled $10Ca(BH_4)_2 + 9MgH_2 + MgF_2$, and $9Ca(BH_4)_2 + Ca(BF_4)_2 + 10MgH_2$ were investigated by in situ SR-PXD. The experiments were performed at the Swiss Norwegian beamline (SNBL) at the European Synchrotron Radiation Facility (ESRF), France (λ = 0.70026 Å, imaging plate system MAR345, 15 s exposure time), and at the beamline I711 of MAX-Lab Synchrotron, Sweden (λ = 0.94608 Å, MAR165 CCD detector, 15 s exposure time). The samples were confined in sapphire capillaries without oxygen contact. In turn, the sapphire capillaries were mounted in a dedicated X-ray diffraction cell for solid−gas reactions, as described elsewhere.[20,21] In-situ hydrogen desorption was performed by heating the samples up to 350 °C with 5 °C min^{-1} heating rate, and kept isothermally at 350 °C under a dynamic vacuum. Two-dimensional powder diffraction data were integrated by the Fit2D program.[22] PXD peak assignment was performed by means of the MAUD software,[23] and the Inorganic Crystal Structure Database (ICSD) was used. Rietveld refinement was performed on selected materials and diffractograms. The Le Bail method with a convergence error of 0.005 was used with the MAUD software for Rietveld refinement.

Samples of cycled $9CaH_2 + CaF_2 + 10MgB_2$ were characterized by high resolution SR-PXD. The patterns were taken at SNBL at the ESRF (λ = 0.50086 Å). Data reduction and peak assignment was performed in the same way as in the in situ SR-PXD.

2.4. DSC Characterization. The DSC characterization was carried out with a Netzsch STA 409 instrument. The measurements were performed in an argon filled glovebox. The samples were heated from room temperature to 500 °C with a heating rate of 5 °C min^{-1} under an argon flow of 50 mL min^{-1}.

3. RESULTS

3.1. First Hydrogenation/Dehydrogenation Cycle. Figure 1 presents the first cycle of hydrogen absorption/desorption of $9CaH_2 + CaF_2 + 10MgB_2$, $10Ca(BH_4)_2 + 9MgH_2 + MgF_2$, and $9Ca(BH_4)_2 + Ca(BF_4)_2 + 10MgH_2$ RHCs. For clarity, it must be mentioned that $9CaH_2 + CaF_2 + 10MgB_2$ composite started at the dehydrogenated state while the two others started in the hydrogenated state. The cycling order was therefore different: absorption then desorption for $9CaH_2 + CaF_2 + 10MgB_2$ and desorption then absorption for the two others. The expected and experimentally achieved hydrogen storage capacity values are collected in Table 1 together with a proposed reaction. The addition of fluorine compounds induced a small change in the absorption/desorption kinetics. The material $9CaH_2 + CaF_2 + 10MgB_2$ presented the highest hydrogen uptake and reversibility during the first cycle.

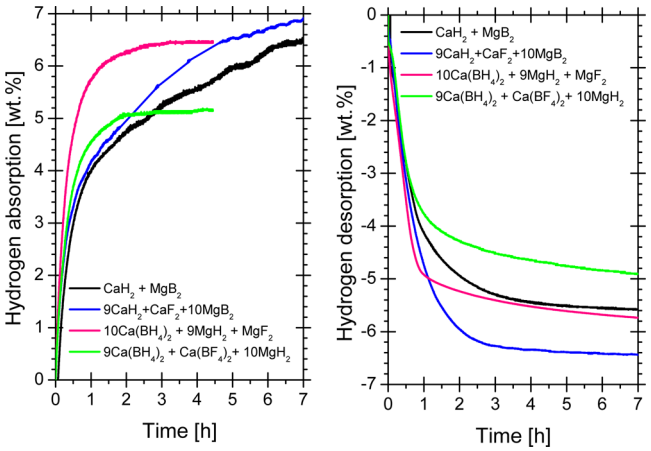

Figure 1. First hydrogen absorption/desorption cycle at $CaH_2 + MgB_2$, $9CaH_2 + CaF_2 + 10MgB_2$, $10Ca(BH_4)_2 + 9MgH_2 + MgF_2$, and $9Ca(BH_4)_2 + Ca(BF_4)_2 + 10MgH_2$ reactive hydride composites.

Figure 2 presents the in situ SR-PXD diffractograms of the dehydrogenation behavior of the $9CaH_2 + 10MgB_2 + CaF_2 - 1ab$ composite. After the hydrogen absorption, the formation of $Ca(BH_4)_2$, MgH_2, and $Ca_4Mg_3H_{14}$ was observed (front of Figure 2, beginning of dehydrogenation experiment). Additionally, peaks of unreacted CaF_2 and MgB_2 and an unidentified peak at 1.6 $Å^{-1}$ were present. During heating, at around 155 °C, the α- to β-$Ca(BH_4)_2$ phase transformation was observed. Furthermore, at this temperature, the formation and fading of a small peak at 1.4 $Å^{-1}$ was observed to take place. The formation

DOI: 10.1021/acs.jpcc.5b01961
J. Phys. Chem. C 2015, 119, 11430−11437

Table 1. Hydrogen Sorption Capacity[a]

proposed reaction[b]	expected H_2 capacity (wt %)	experimental H_2 uptake (wt %)	experimental H_2 release (wt %)
CaH_2 + MgB_2 + $4H_2$ ↔ $Ca(BH_4)_2$ + MgH_2	8.3	6.5[c]	5.6[c]
$9CaH_2$ + CaF_2 + $10MgB_2$ + $36H_2$ ↔ $9Ca(BH_4)_2$ + $9MgH_2$ + MgB_2 + CaF_2[d]	7.2	6.8[c]	6.4[c]
$10Ca(BH_4)_2$ + $9MgH_2$ + MgF_2 → $9CaH_2$ + CaF_2 + $10MgB_2$ + $40H_2$	8.0	6.5[e]	5.7[e]
$9Ca(BH_4)_2$ + $Ca(BF_4)_2$ + $10MgH_2$ → $6CaH_2$ + $4CaF_2$ + $10MgB_2$ + $40H_2$	7.2	5.1[e]	4.9[e]

[a]Absorption 130 bar H_2 pressure and 350 °C, desorption 0.1 bar H_2 and pressure 350 °C. [b]Bold type: as prepared ball milled materials. [c]Absorption then desorption. [d]Consistent with a cubic solid solution CaF_2−CaH_2 (see Table 2). [e]Desorption then absorption.

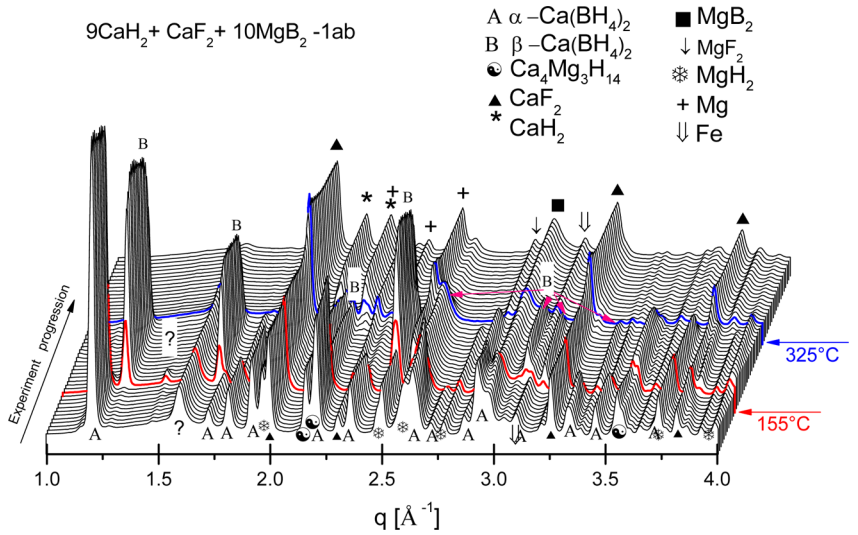

Figure 2. In situ SR-PXD dehydrogenation of $9CaH_2$ + CaF_2 + $10MgB_2$ − 1ab RHC (5 °C min^{-1}, SNBL-ERSF, λ = 0.70026 Å).

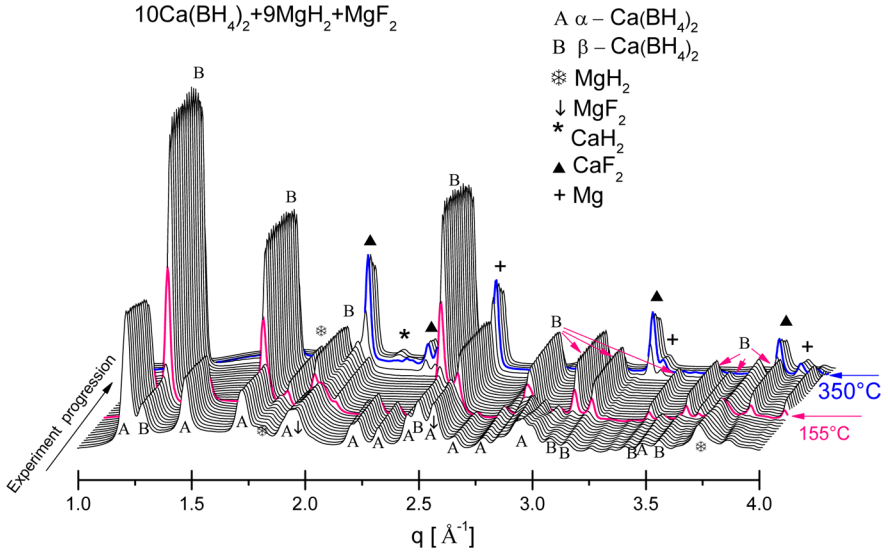

Figure 3. In situ SR-PXD dehydrogenation of $10Ca(BH_4)_2$ + $9MgH_2$ + MgF_2 RHC (5 °C min^{-1}, SNBL-ERSF, λ = 0.70026 Å).

of CaH_2 started at around 325 °C; meanwhile, the intensities of CaF_2 and MgB_2 peaks increased. The CaF_2 peaks were consistent with a cubic solid solution CaF_2−CaH_2; this will be discussed in detail below. Simultaneously, the peak intensity of the hydrogenated phases β-$Ca(BH_4)_2$ and MgH_2 decreased. During the isothermal period at 350 °C, the peaks of $Ca_4Mg_3H_{14}$ and the unidentified peak at 1.6 $Å^{-1}$ disappeared. After the dehydrogenation reaction, the presence of CaF_2, MgB_2, CaH_2, Mg, small quantities of MgF_2, and Fe (from milling vial) was observed.

The in situ SR-PXD analysis of the dehydrogenation process of $10Ca(BH_4)_2$ + $9MgH_2$ + MgF_2 is presented in Figure 3. The as milled material (front of Figure 3) presented peaks corresponding to α-$Ca(BH_4)_2$, MgH_2, and MgF_2. The α- to β-$Ca(BH_4)_2$ phase transition occurred around 155 °C. At 350 °C, the peaks corresponding to β-$Ca(BH_4)_2$, MgH_2, and MgF_2 vanished, while peaks of CaF_2, CaH_2, and Mg developed. CaF_2,

DOI: 10.1021/acs.jpcc.5b01961
J. Phys. Chem. C 2015, 119, 11430−11437

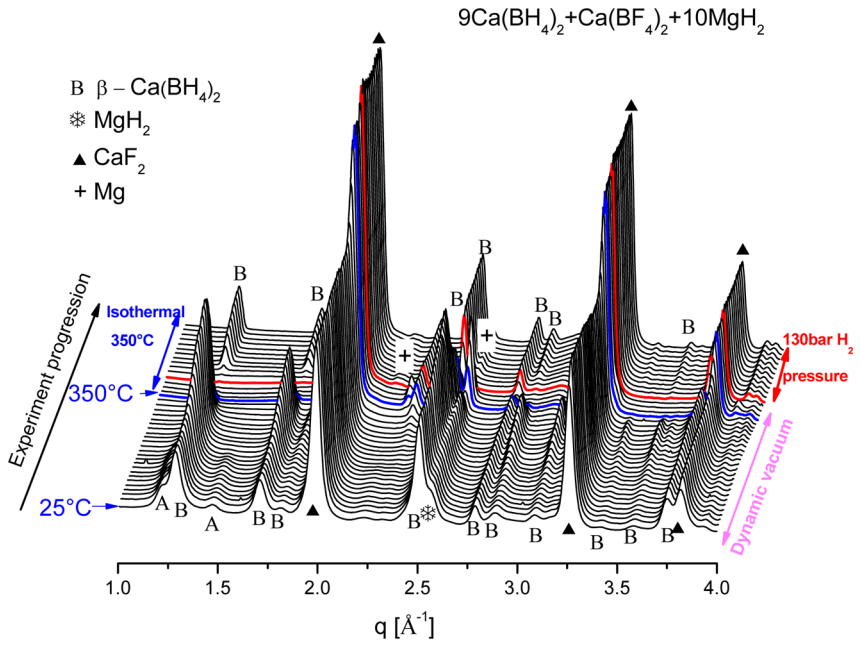

Figure 4. In situ SR-PXD first dehydrogenation and rehydrogenation behavior of $9Ca(BH_4)_2 + Ca(BF_4)_2 + 10MgH_2$ RHC (5 °C min^{-1}, λ = 0.94608 Å, Max Lab).

not present in the initial mixture, was formed during the dehydrogenation reaction (back of Figure 3). This indicates a change of F bonding during the solid−gas reactions. The formation of CaF_2 is favored thermodynamically, ΔH^f_{298} = −1229.3 kJ mol^{-1}, versus MgF_2 ΔH^f_{298} = −1124 kJ mol^{-1}.[24]

The dehydrogenation reaction of as milled $9Ca(BH_4)_2 + Ca(BF_4)_2 + 10MgH_2$ is shown in Figure 4. In this RHC, the formation of CaF_2 was observed after milling and there was no indication of any remaining $Ca(BF_4)_2$. Interestingly, after ball milling, the high temperature β-$Ca(BH_4)_2$ phase was found at room temperature. The dehydrogenation reaction of both MgH_2 and β-$Ca(BH_4)_2$ finished at 350 °C. Instead of the expected MgB_2 phase, metallic Mg was formed after dehydrogenation. In the same setup, the H_2 pressure was changed from dynamic vacuum to 130 bar under isothermal conditions (i.e., 350 °C). Then, the rehydrogenation reaction was observed. The main phases in the rehydrogenated system determined by in situ SR-PXD were β-$Ca(BH_4)_2$, MgH_2, and CaF_2.

DSC-dehydrogenation profiles are presented in Figure 5. In addition to the studied RHCs, the reference materials $Ca(BH_4)_2 + MgH_2$, hydrogenated $CaH_2 + MgB_2$ (hereafter $CaH_2 + MgB_2$ − 1ab), as-received $Ca(BF_4)_2{\cdot}xH_2O$, and $9MgH_2 + MgF_2$ ball milled mixture were analyzed. The reference materials, $Ca(BH_4)_2 + MgH_2$ (frame a) and $CaH_2 + MgB_2$ − 1ab (frame b), showed different behavior. The $CaH_2 + MgB_2$ − 1ab presented three peaks shifted to higher temperatures as compared with one-peak $Ca(BH_4)_2 + MgH_2$. The addition of CaF_2 as an additive to $CaH_2 + MgB_2$ (frame c) led to a 10 °C decrease in the dehydrogenation temperature peak, compared to the materials without an additive (frames a and b). The DSC of the $9MgH_2 + MgF_2$ mixture (frame d) presented a peak dehydrogenation temperature lower than the RHCs tested, suggesting that the $Ca(BH_4)_2$ dominates the dehydrogenation process. The composite $10Ca(BH_4)_2 + 9MgH_2 + MgF_2$ (frame e) presented an increase of dehydrogenation temperature compared to the $9MgH_2 + MgF_2$ mixture but within the range of the studied Ca-based RHCs. In the DSC data of $9Ca(BH_4)_2 + Ca(BF_4)_2 + 10MgH_2$ (frame g), the main peak of dehydrogenation was shifted to higher temperatures than the referenced materials and it was surrounded by two shoulders.

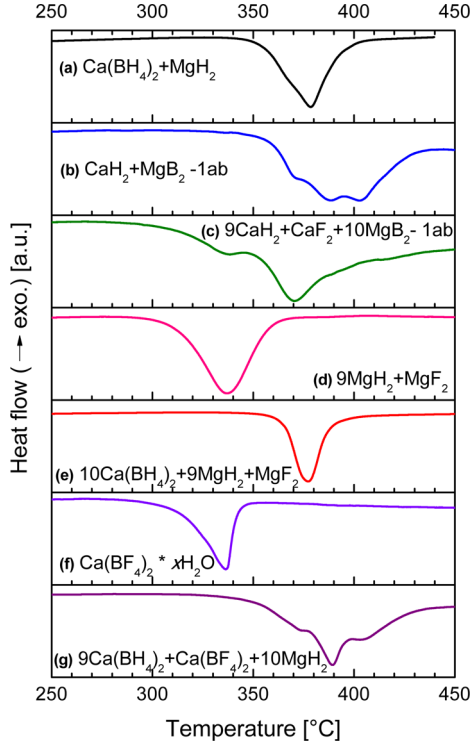

Figure 5. DSC profiles of first dehydrogenation of reactive hydride composites and references, measured at 5 °C min^{-1} heating rate.

3.2. Second Hydrogenation/Dehydrogenation Cycle.

Figure 6 presents the two-cycle testing of $9CaH_2 + CaF_2 + 10MgB_2$. At the successive cycling, a progressive reduction was demonstrated in the hydrogen uptake and release. After the second hydrogen desorption, just about 4 wt % of hydrogen was released. Figure 7 shows the high resolution SR-PXD

DOI: 10.1021/acs.jpcc.5b01961
J. Phys. Chem. C 2015, 119, 11430−11437

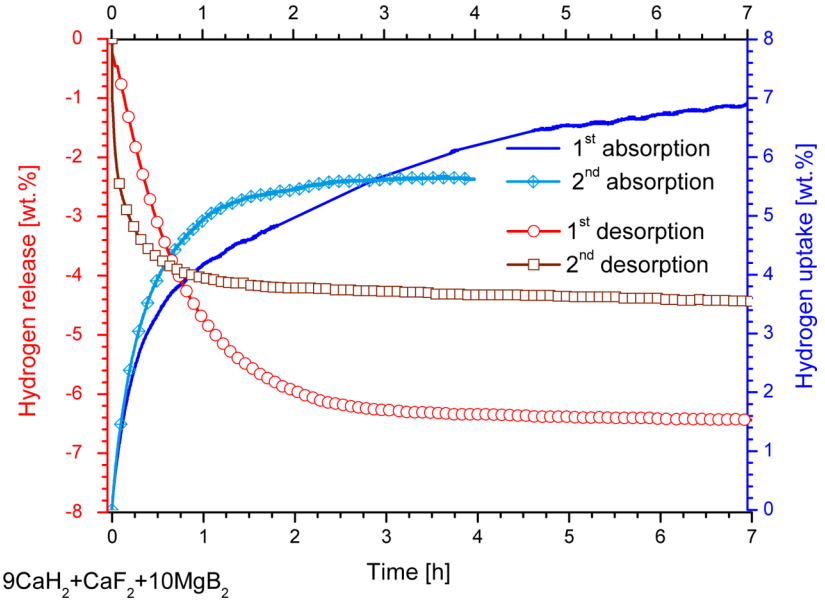

Figure 6. Two hydrogen absorption/desorption cycles of $9CaH_2 + CaF_2 + 10MgB_2$ RHC.

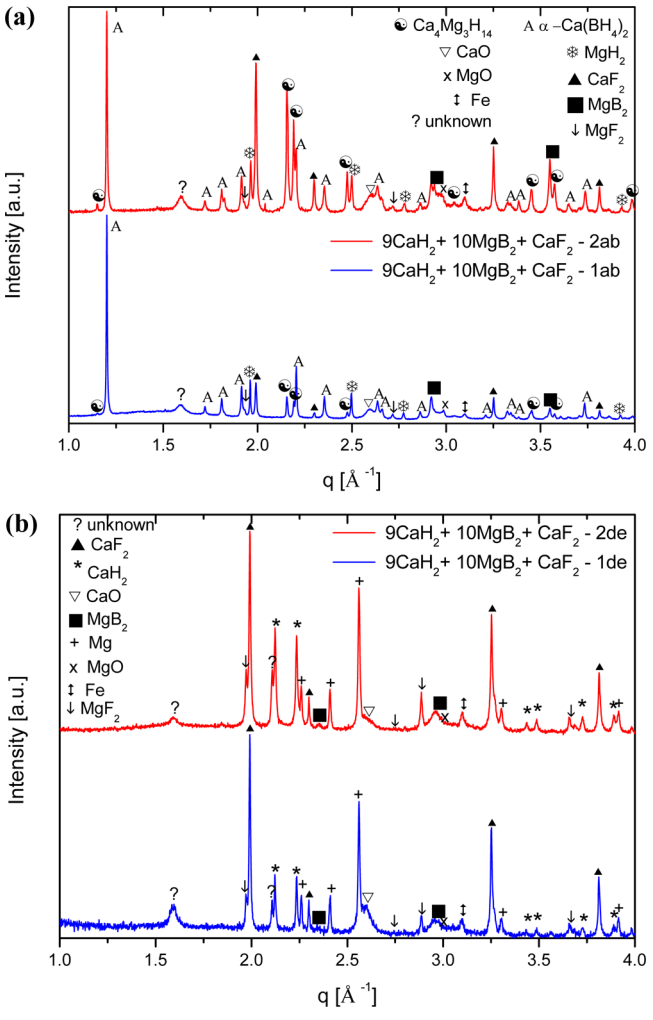

Figure 7. (a) High resolution SR-PXD patterns of the first and second absorption states of $CaF_2 + 9CaH_2 + 10MgB_2$ (SNBL-ERSF, λ = 0.50086 Å). (b) High resolution SR-PXD patterns of the first and second dehydrogenated states of $CaF_2 + 9CaH_2 + 10MgB_2$ (SNBL-ERSF, λ = 0.50086 Å).

patterns of the first and second absorption states of the $9CaH_2 + CaF_2 + 10MgB_2$ RHC. The main hydrogenation products (Figure 7a) were $Ca(BH_4)_2$ and MgH_2. In addition to the main products, $Ca_4Mg_3H_{14}$, CaF_2, MgB_2, the small amount of MgF_2, and small contaminations of Fe, CaO, and MgO were also present in the sample. The second hydrogenation pattern showed an increase of $Ca_4Mg_3H_{14}$ peak intensity. The main dehydrogenation products of $9CaH_2 + CaF_2 + 10MgB_2$ RHC (Figure 7b) were CaH_2, CaF_2, MgB_2, Mg, and MgF_2.

Figure 8 collects the SR-PXD diffractograms of the as-milled $9CaH_2-CaF_2$, the last diffractogram of in situ SR-PXD

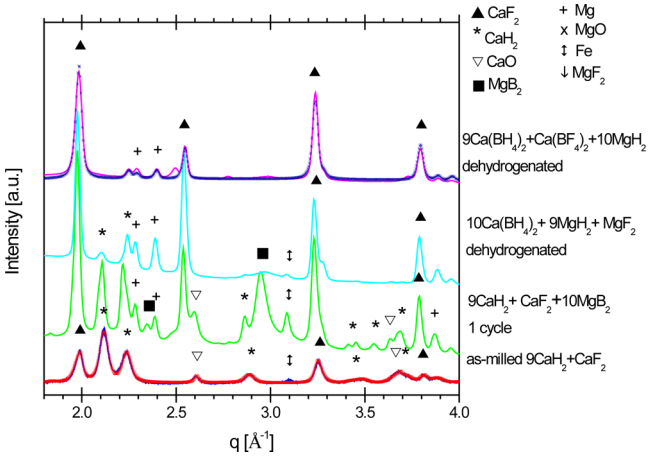

Figure 8. SR-PXD patterns of as-milled $9CaH_2 + CaF_2$, one-cycled $9CaH_2 + CaF_2 + 10MgB_2$, dehydrogenated $10Ca(BH_4)_2 + 9MgH_2 + MgF_2$, and dehydrogenated $9Ca(BH_4)_2 + Ca(BF_4)_2 + 10MgH_2$ showing the progressive change from orthorhombic to cubic CaH_2-CaF_2 transformation. Line: experimental. Dots: refined data.

dehydrogenation of $9CaH_2 + CaF_2 + 10MgB_2$ − 1ab (corresponding to $9CaH_2 + CaF_2 + 10MgB_2$ cycled one time), the last diffractogram of in situ SR-PXD dehydrogenation of $10(CaBH_4)_2 + 9MgH_2 + MgF_2$, and the last diffractogram of the in situ SR-PXD dehydrogenation part of $9(CaBH_4)_2 + Ca(BF_4)_2 + 10MgH_2$. All of them represent

DOI: 10.1021/acs.jpcc.5b01961
J. Phys. Chem. C 2015, 119, 11430−11437

Table 2. Refinement Unit Cell Parameters of CaF_2 and CaH_2[a]

material	CaH_2 refined unit cell parameters (Å) [reported cell lattice (Å), ICSD-155987, a = 5.899; b = 3.570; c = 6.769]	CaF_2 refined unit cell parameter (Å) [reported cell lattice (Å), ICSD-82707, a = 5.4712(4)]
as-milled $9CaH_2 + 1CaF_2$	a = 5.965(1) b = 3.606(1) c = 6.843(2)	a = 5.472(1)
dehydrogenated $9Ca(BH_4)_2 + Ca(BF_4)_2 + 10MgH_2$		a = 5.508(2)

[a]Estimated standard deviations in parentheses.

dehydrogenated materials where CaF_2, CaH_2, and MgB_2 are present but with differences. The peak intensity of CaH_2 and MgB_2 reduced in the order $9CaH_2 + CaF_2 + 10MgB_2$ cycled one time > dehydrogenated $10(CaBH_4)_2 + 9MgH_2 + MgF_2$ > dehydrogenated $9(CaBH_4)_2 + Ca(BF_4)_2 + 10MgH_2$; meanwhile, the CaF_2 peak intensity increased (relative peak intensity). Rietveld refinement was performed for as-milled $9CaH_2$–CaF_2 and dehydrogenated $9(CaBH_4)_2 + Ca(BF_4)_2 + 10MgH_2$ to check for the formation of CaF_2–CaH_2 solid solution; thermal effects were taken into consideration. For the as-milled $9CaH_2$–CaF_2, an enlarged orthorhombic CaH_2 structure dominates. For the Ca-RHC, an enlarged cubic CaF_2 was found. Both states are consistent with the formation of solid solutions of CaF_2–CaH_2 (Table 2).[25]

4. DISCUSSION

4.1. Kinetic Considerations. The absorption/desorption experiments indicate a lower than expected hydrogen uptake and a progressive reduction in the reversible hydrogen storage capacity upon cycling. The reduction in the reversibility can be associated with the formation of $Ca_4Mg_3H_{14}$ during hydrogenation and the formation of Mg at the dehydrogenation, both observed here by SR-PXD. The dehydrogenation conditions are adequate to decompose $Ca_4Mg_3H_{14}$, but its dehydrogenation leads to the formation of Mg instead of MgB_2, decreasing the overall cycle capability of the system. The formation of unreactive species such as amorphous boron or nanocrystalline $CaB_{12}H_{12}$ is another factor to be considered. The formation of unreactive B-compounds was already observed in the $Ca(BH_4)_2$, $Ca(BH_4)_2 + MgH_2$, and $CaH_2 + MgB_2$ systems.[3,6,26] The formation of unreactive B-compounds is responsible for the decrease of B available to form $Ca(BH_4)_2$ and MgB_2. In the present work, no crystalline B-compounds were observed. However, we cannot discard the possible formation of amorphous B-compounds. All together, the formation of $Ca_4Mg_3H_{14}$, Mg, and unreactive B-compounds represents a major problem in Ca-RHCs.

4.2. Thermodynamic Considerations. As commented in the Results section, depending on the F-source, there was a change of F bonding during the solid–gas reactions and the formation of CaF_2 was favored due to its high thermodynamic stability. The formation of crystalline $Ca_4Mg_3H_{14}$ was also affected according to the F-source. For the $9CaH_2 + 10MgB_2 + CaF_2$ – 1ab, the presence of $Ca_4Mg_3H_{14}$ was clear. However, for the $10Ca(BH_4)_2 + 9MgH_2 + MgF_2$ and particularly for the $9Ca(BH_4)_2 + Ca(BF_4)_2 + 10MgH_2$, where both hydrogenation and dehydrogenation were performed in a single in situ experiment, the formation of crystalline $Ca_4Mg_3H_{14}$ was not evident. The $Ca_4Mg_3H_{14}$ appearance on Ca–Mg–H systems[6,17,19] suggests that $Ca_4Mg_3H_{14}$ must be a thermodynamic stable ternary hydride. From our observations and reported data,[19] this material decomposes between 325 and 350 °C at 0–1 bar H_2. The formation of $Ca_4Mg_3H_{14}$ was first reported, together with its crystal structure by Gingl et al. in 1992.[27] Posterior reviews on hydrogen storage materials report its existence and possible hydrogen storage use,[28] the detailed material crystal structure,[29] but none about thermodynamic data. This ternary hydride is relatively new and unstudied for hydrogen storage; to the best of our knowledge, no experimental or theoretical/computational thermodynamic data is available to verify our observations on formation and decomposition. Other RHCs also show a competition between the formation of the RHC products, i.e., borohydrides and magnesium hydride, and magnesium ternary hydrides during hydrogenation. For example, Garroni et al. have shown the formation of $NaMgH_3$ as high as 18 wt % in the system $NaBH_4 + 2MgH_2$[30] and a lowering in the hydrogen uptake.

4.3. Structural Considerations. The dehydrogenation of the three studied Ca-RHCs reveals a sudden increase of CaF_2 peak intensity simultaneous with the disappearance of β-$Ca(BH_4)_2/MgH_2$ peaks. The in situ rehydrogenation of $9Ca(BH_4)_2 + Ca(BF_4)_2 + 10MgH_2$ did not show a reduction of CaF_2 peak intensity, indicating that the CaF_2 did not re-enter in the RHC reaction scheme as wanted. Initially, the CaF_2 was connected to the RHC scheme via the formation of an orthorhombic solid solution CaF_2–CaH_2 produced during ball milling, already reported as $CaF_{2-x}H_x$.[25] As-milled $9CaH_2 + CaF_2$, one-cycled $9CaH_2 + CaF_2 + 10MgB_2$, dehydrogenated $10Ca(BH_4)_2 + 9MgH_2 + MgF_2$, and dehydrogenated $9Ca(BH_4)_2 + Ca(BF_4)_2 + 10MgH_2$ (Figure 8) reveal the changes in the solid solution upon heating and hydrogen exposure. As mentioned above, as-milled $9CaH_2 + CaF_2$ is a partial orthorhombic solid solution with the main structure of orthorhombic CaH_2; meanwhile, cycled $9CaH_2 + CaF_2 + 10MgB_2$, dehydrogenated $10Ca(BH_4)_2 + 9MgH_2 + MgF_2$, and dehydrogenated $9Ca(BH_4)_2 + Ca(BF_4)_2 + 10MgH_2$ presented an enlarged structure of cubic CaF_2, consistent with the formation of a cubic CaF_2–CaH_2 solid solution (refined unit cell axis of the two extreme cases in Table 2). The formation of a solid solution of $CaF_{2-x}H_x$ has been proposed as a possible way to tune the thermodynamics of hydrogen desorption.[25] In this regard, there are two possibilities, the formation of the cubic solid solution (CaH_2 into CaF_2) or the orthorhombic solid solution (CaF_2 into CaH_2), with different enthalpies of mixing, negative and positive, respectively.[25] It has been proposed that the enthalpy of mixing can change the decomposition temperature.[15,25] Lee et al. proposed that the heat of mixing of CaF_2–CaH_2 in the related system, $^3/_2Ca(BH_4)_2 + CaX_2 \leftrightarrow 2CaHX + {}^1/_2CaB_6 + 5H_2$, leads to a small decrease of the equilibrium temperature. The DSC measurements shown in this work (Figure 5) demonstrate a 10 °C reduction in the peak dehydrogenation temperature of $9CaH_2 + CaF_2 + 10MgB_2$ – 1ab as compared to $Ca(BH_4)_2 + MgH_2$.

DOI: 10.1021/acs.jpcc.5b01961
J. Phys. Chem. C 2015, 119, 11430–11437

However, this reduction of dehydrogenation temperature is far away from the target.

The formation of the $CaF_{2-x}H_x$ solid solution has been proposed as having a detrimental effect by reducing the availability of CaH_2 to form $Ca(BH_4)_2$ upon cycling.[19] This is consistent with the observed reduction of the hydrogen uptake and release. Additionally, the increase of $Ca_4Mg_3H_{14}$ and decrease of $Ca(BH_4)_2$ upon cycling, as observed by high resolution SR-PXD, is a major disadvantage for the RHC.

CONCLUSIONS

Several compositions of Ca-RHC with different sources of fluorine were prepared by ball milling and tested for hydrogen uptake. Among the tested Ca-RHCs, the $9CaH_2 + CaF_2 + 10MgB_2$ presented the highest hydrogen storage capacity. Despite the elegant idea behind the Ca-based reactive hydride composites, the experimental results indicate that the theoretical dehydrogenation temperature and the expected reversibility were not achieved. The reasons for this include the formation of the ternary hydride $Ca_4Mg_3H_{14}$ during hydrogenation and the formation of Mg instead of MgB_2 during dehydrogenation.

The addition of the fluorinated compounds modified the dehydrogenation pathway. Independently of the fluorine source, CaF_2 was formed during dehydrogenation reactions. CaF_2 was found as part of CaF_2–CaH_2 solid solutions, as evident from shifts in the unit cell parameters.

AUTHOR INFORMATION

Corresponding Author

*Phone: +52 55 5623-7300, ext 80548. E-mail: karina_suarez@iim.unam.mx.

Notes

The authors declare no competing financial interest.

ACKNOWLEDGMENTS

The authors appreciate the financial support from the European Community in the frame of integrated project "FLYHY - Fluorine Substituted High Capacity Hydrides for Hydrogen Storage at low Working Temperatures" (Grant agreement no.: N° 226943-2). The authors appreciate the facilities and technical support at 711 beamline of MAX-lab Synchrotron, especially Dörthe Haase. The authors thank the project team at SNBL at the ESRF, France, for their skillful assistance.

REFERENCES

(1) Stetson, N. T.; Bowman, R. C., Jr.; Olson, G. L. Overview of Hydrogen Storage, Transportation, Handling and Distribution. In *Handbook of Hydrogen Energy*; Sherif. S. A., Yogi-Goswami, D., Stefanakos, E. K., Steinfeld, A., Eds.; CRC Press: Boca Raton, FL, 2014.

(2) Yang, J.; Sudik, A.; Wolverton, C.; Siegel, D. J. High Capacity Hydrogen Storage Materials: Attributes for Automotive Applications and Techniques for Materials Discovery. *Chem. Soc. Rev.* **2010**, *39*, 656–675.

(3) Chandan, A.; Hattenberger, M.; El-kharouf, A.; Du, S.; Dhir, A.; Self, V.; Pollet, B. G.; Ingrama, A.; Bujalski, W. A High Temperature (HT) Polymer Electrolyte Membrane Fuel Cells (PEMFC) - A Review. *J. Power Sources* **2013**, *231*, 264–278.

(4) Guo, Z.; Xu, X.; Xiang, Y.; Lu, S.; Ping-Jiang, S. New Anhydrous Proton Exchange Membranes for High-Temperature Fuel Cells Based on PVDF–PVP Blended Polymers. *J. Mater. Chem. A* **2015**, *3*, 148–155.

(5) Vajo, J. J.; Skeith, S. L.; Mertens, F. Reversible Storage of Hydrogen in Destabilized $LiBH_4$. *J. Phys. Chem. B* **2005**, *109*, 3719–3722.

(6) Barkhordarian, G.; Klassen, T.; Dornheim, M.; Bormann, R. Unexpected Kinetic Effect of MgB_2 in Reactive Hydride Composites Containing Complex Borohydrides. *J. Alloys Compd.* **2007**, *440*, L18–L21.

(7) Barkhordarian, G.; Jensen, T. R.; Doppiu, S.; Boesenberg, U.; Borgschulte, A.; Gremaud, R.; Cerenius, Y.; Dornheim, M.; Klassen, T.; Bormann, R. Formation of $Ca(BH_4)_2$ from Hydrogenation of CaH_2+MgB_2 Composite. *J. Phys. Chem. C* **2008**, *112*, 2743–2749.

(8) Siegel, D. J.; Wolverton, C.; Ozolins, V. Thermodynamic Guidelines for the Prediction of Hydrogen Storage Reactions and Their Application to Destabilized Hydride Mixtures. *Phys. Rev. B* **2007**, *76*, 134102-6.

(9) Bösenberg, U.; Kim, J. W.; Gosslar, D.; Eigen, N.; Jensen, T. R.; Bellosta von Colbe, J. M.; Zhou, Y.; Dahms, M.; Kim, D. H.; Gunther, R.; et al. Role of Additives in $LiBH_4$–MgH_2 Reactive Hydride Composites for Sorption Kinetics. *Acta Mater.* **2010**, *58*, 3381–3389.

(10) Bonatto-Minella, C.; Garroni, S.; Pistidda, C.; Gosalawit-Utke, R.; Barkhordarian, G.; Rongeat, C.; Lindemann, I.; Gutfleisch, O.; Jensen, T. R.; Cerenius, Y.; et al. Effect of Transition Metal Fluorides on the Sorption Properties and Reversible Formation of $Ca(BH_4)_2$. *J. Phys. Chem. C* **2011**, *115*, 2497–2504.

(11) Eigen, N.; Bösenberg, U.; Bellosta von Colbe, J.; Jensen, T. R.; Cerenius, Y.; Dornheim, M.; Klassen, T.; Bormann, R. Reversible Hydrogen Storage in NaF–Al Composites. *J. Alloys Compd.* **2009**, *477*, 76–80.

(12) Gosalawit, R.; Bellosta von Colbe, J. M.; Dornheim, M.; Jensen, T. R.; Cerenius, Y.; Bonatto, C. M.; Peschke, M.; Bormann, R. LiF–MgB_2 System for Reversible Hydrogen Storage. *J. Phys. Chem. C* **2010**, *114*, 10291–10296.

(13) Saldan, I.; Gosalawit-Utke, R.; Pistidda, C.; Bösenberg, U.; Schulze, M.; Jensen, T. R.; Taube, K.; Dornheim, M.; Klassen, T. Influence of Stoichiometry on the Hydrogen Sorption Behaviour in the LiF–MgB_2 System. *J. Phys. Chem. C* **2012**, *116*, 7010–7015.

(14) Saldan, I.; Ramallo-López, J. M.; Requejo, F. G.; Suarez-Alcantara, K.; Bellosta von Colbe, J.; Avila, J. NEXAFS Study of 2LiF–MgB_2 Composite. *Int. J. Hydrogen Energy* **2012**, *37*, 10236–10239.

(15) Lee, J. Y.; Lee, Y. S.; Suh, J. Y.; Shim, J. H.; Cho, Y. W. Metal Halide Doped Metal Borohydrides for Hydrogen Storage: The Case of $Ca(BH_4)_2$–CaX_2 (X = F, Cl) Mixture. *J. Alloys Compd.* **2010**, *506*, 721–727.

(16) Gosalawit-Utke, R.; Suarez, K.; Bellosta von Colbe, J. M.; Bösenberg, U.; Jensen, T. R.; Cerenius, Y.; Bonatto Minella, C.; Pistidda, C.; Barkhordarian, G.; Schulze, M.; et al. $Ca(BH_4)_2$-MgF_2 Reversible Hydrogen Storage: Reaction Mechanisms and Kinetic Properties. *J. Phys. Chem. C* **2011**, *115*, 3762–3768.

(17) Suarez-Alcantara, K.; Ramallo-Lopez, J. M.; Bösenberg, U.; Saldan, I.; Pistidda, C.; Requejo, F. G.; Jensen, T.; Cerenius, Y.; Sørby, M.; Avila, J.; et al. $3CaH_2 + 4MgB_2 + CaF_2$ Reactive Hydride Composite as a Potential Hydrogen Storage Material: Hydrogenation and Dehydrogenation Pathway. *J. Phys. Chem. C* **2012**, *116*, 7207–7212.

(18) Suarez-Alcantara, K.; Bösenberg, U.; Zavorotynska, O.; Bellosta von Colbe, J.; Taube, K.; Baricco, M.; Klassen, T.; Dornheim, M. Sorption and Desorption Properties of a $CaH_2/MgB_2/CaF_2$ Reactive Hydride Composite as Potential Hydrogen Storage Material. *J. Solid State Chem.* **2011**, *184*, 3104–3109.

(19) Pistidda, C.; Karimi, F.; Garroni, S.; Rzeszutek, A.; Bonatto Minella, C.; Milanese, C.; Le, T. T.; Rude, L. H.; Skibsted, J.; Jensen, T. R.; et al. Effect of the Partial Replacement of CaH_2 with CaF_2 in the Mixed System $CaH_2 + MgB_2$. *J. Phys. Chem. C* **2014**, *118*, 28409–28417.

(20) Jensen, T. R.; Nielsen, T. K.; Filinchuk, Y.; Jørgensen, J. E.; Cerenius, Y.; Gray, E. M.; Webb, C. J. Versatile in Situ Powder X-ray Diffraction Cells for Solid–Gas Investigations. *J. Appl. Crystallogr.* **2010**, *43*, 1456–1463.

DOI: 10.1021/acs.jpcc.5b01961
J. Phys. Chem. C 2015, 119, 11430–11437

(21) Bösenberg, U.; Pistidda, C.; Tolkiehn, M.; Busch, N.; Saldan, I.; Suarez-Alcantara, K.; Arendarska, A.; Klassen, T.; Dornheim, M. Characterization of Metal Hydrides by in-Situ XRD. *Int. J. Hydrogen Energy* **2014**, *39*, 9899−9903.
(22) Hammersley, A. P. FIT2D V12.077. Internal Report ESRF-97-HA02 T, 1997.
(23) Lutterotti, L.; Matthies, S.; Wenk, H. R. MAUD: a Friendly Java Program for Material Analysis Using Diffraction. *International Union of Crystallography: Newsletter of the Commission for Powder Diffraction* **1999**, *21*, 14−15.
(24) Kubaschewski, O.; Alcock, C. B.; Spencer, P. J. *Materials Thermochemistry*, 6th ed.; Pergamon Press, New York, 1993.
(25) Pinatel, E. R.; Rude, L. H.; Corno, M.; Kragelund, M.; Ugliengo, P.; Jensen, T. R.; Baricco, M. Thermodynamic Tunning of Calcium Hydride by Fluoride Substitution. *Mater. Res. Soc. Symp. Proc.* **2012**, *1441*, 943−6.
(26) Hawang, S. J.; Bowman, R. C., Jr.; Reiter, J. W.; Rijssenbeek, J.; Soloveichik, G. L.; Zhao, J. C.; Kabbour, H.; Ahn, C. C. NMR Confirmation for Formation of $[B_{12}H_{12}]^{2-}$ Complexes During Hydrogen Desorption from Metal Borohydrides. *J. Phys. Chem. C* **2008**, *112*, 3164−3169.
(27) Gingl, F.; Bonhomme, F.; Yvon, K. Tetracalcium Trimagnesium Tetradecahydride, $Ca_4Mg_3H_{14}$: the First Ternary Alkaline Earth Hydride. *J. Alloys Compd.* **1992**, *185*, 273−278.
(28) Grochala, W.; Edwards, P. P. Thermal Decomposition of the Non-Interstitial Hydrides for the Storage and Production of Hydrogen. *Chem. Rev.* **2004**, *104*, 1283−1315.
(29) Yvon, K.; Bertheville, B. Magnesium Based Ternary Metal Hydrides Containing Alkali and Alkaline-Earth Elements. *J. Alloys Compd.* **2006**, *425*, 101−108.
(30) Garroni, S.; Milanese, C.; Girella, A.; Marini, A.; Mulas, G.; Menendez, E.; Pistidda, C.; Dornheim, M.; Surinach, S.; Baro, M. D. *Int. J. Hydrogen Energy* **2010**, *35*, 5434−5441.

DOI: 10.1021/acs.jpcc.5b01961
J. Phys. Chem. C 2015, 119, 11430−11437